EPR and ENDOR Investigation of the Primary Electron Acceptor Radical Anion $Q_A^{\bullet -}$ in Iron-Depleted Photosystem II Membrane Fragments†

Fraser MacMillan, Friedhelm Lendzian, Gernot Renger, and Wolfgang Lubitz*

Max-Volmer-Institut für Biophysikalische und Physikalische Chemie, Technische Universität Berlin, Berlin, Germany

Received December 28, 1994; Revised Manuscript Received April 5, 1995⊗

ABSTRACT: Photosystem II (PS II) membrane fragments were treated with trypsin at pH = 7.4 followed by incubation with *o*-phenanthroline and lithium perchlorate. This procedure removes and/or decouples the non-heme Fe^{2+} associated with the quinones Q_A and Q_B in the PS II reaction center (RC). Treatment of such samples (referred to as iron-depleted) with sodium dithionite or illumination in the presence of dichlorophenol indophenol (DCIP) and sodium ascorbate yielded EPR spectra similar to those of the plastoquinone-9 (PQ-9) radical anion generated in organic solvents. Q-band EPR yielded the principal values of the *g*-tensor for $PQ\text{-}9^{\bullet -}$ in 2-propanol and $Q_A^{\bullet -}$ in PS II. Electron nuclear double resonance (ENDOR) experiments were performed both on $PQ\text{-}9^{\bullet -}$ *in vitro* and on $Q_A^{\bullet -}$ in the iron-depleted PS II samples. For the former a complete set of isotropic ^1H hyperfine coupling constants and hyperfine tensors of the two methyl groups and the α-proton were obtained. On the basis of H/D exchange experiments two different hydrogen bonds could be detected in frozen solution that are formed between the carbonyl oxygens of the radical and protons from the surrounding solvent molecules. The hydrogen bond distances were estimated using the point-dipole model. ^1H-ENDOR spectra of $Q_A^{\bullet -}$ in iron-depleted PS II samples have been measured in buffers made in H_2O and D_2O. The spectrum in deuterated buffer allowed the determination of two different methyl group hyperfine tensors. Differences detected between the spectra in protonated and deuterated buffer reveal the hyperfine tensors of two exchangeable protons belonging to hydrogen bonds between the oxygens of Q_A and specific protein residues. The assignment of these hydrogen bonds in PS II is discussed and compared with the situation found in the bacterial reaction center.

Water cleavage in photosystem II (PS II)[1] by visible light leads to formation of molecular dioxygen released into the atmosphere and bound hydrogen in the form of plastoquinol (PQH_2); for a recent review, see Renger (1993). The latter process takes place in a special protein pocket referred to as the Q_B site where a non-covalently bound plastoquinone molecule from a plastoquinone pool becomes reduced to plastoquinol via a sequence of two univalent electron-transfer steps by a special plastosemiquinone, $Q_A^{\bullet -}$, acting as the donor. The functional (Crofts & Wraight, 1983) and structural (Michel & Deisenhofer, 1988) organization of this process closely resembles that of the ubiquinol formation in anoxygenic purple bacteria. In both types of reaction centers (RCs), a high-spin non-heme iron is located between Q_A and Q_B. In the purple bacteria RC, this metal center is known (Deisenhofer & Michel, 1988; Feher et al., 1989) to be coordinated by four histidine residues (two from each of the L and M subunits of the heterodimer forming the RC apoprotein) and a glutamate. An analogous ligation by four histidines from polypeptides D1 and D2 is assumed to bind the non-heme iron in the PS II complex (Michel & Deisenhofer, 1988; Trebst, 1986). Recently, one of these histidine ligands was replaced by glutamine using site-directed mutagenesis (Vermaas et al., 1994). This resulted in a dramatic decrease of the quantum efficiency of Q_A reduction. The Fe^{2+} was shown to be decoupled from Q_A or even removed from PS II.

On the other hand, there are marked differences in the properties of the Fe^{2+} between purple bacteria and PS II: (i) the redox potential of the couple Fe^{2+}/Fe^{3+} is significantly lower in PS II (Bowes et al., 1979; Petrouleas & Diner, 1986; Renger et al., 1987); and (ii) glutamate acts as a bidentate ligand in purple bacteria, whereas bicarbonate is likely to be coordinated with Fe^{2+} in PS II (Govindjee & van Rensen, 1994, and references therein).

The functional role of the non-heme iron center is not yet fully understood. Regardless of this problem, the presence of a high-spin transition metal center gives rise to magnetic interactions with the spin states of other nearby redox groups and thereby profoundly affects the application of magnetic resonance methods as an analytical tool in studying the electronic structure of redox components located in PS II. It was shown that the Fe^{2+} can be reversibly removed from bacterial RCs (Debus et al., 1986) and replaced by other metal ions, e.g., Zn^{2+}. This procedure has been used in order to permit successful measurements of EPR and in particular ENDOR spectra of $Q_A^{\bullet -}$ and to gather information on the microenvironment of $Q_A^{\bullet -}$, especially of hydrogen bond

†This work was supported by Deutsche Forschungsgemeinschaft (Sfb 312, TP A2 and A4) and by Fonds der Chemischen Industrie (W.L.)

* To whom correspondence should be addressed; Max-Volmer-Institut für Biophysikalische und Physikalische Chemie, PC 14, Technische Universität Berlin, Strasse des 17.Juni 135, D-10623 Berlin, Germany. Fax: (#49 30) 31 42 11 22.

⊗ Abstract published in *Advance ACS Abstracts,* May 15, 1995.

[1] Abbreviations: PS II, photosystem II; Q_A, first quinone electron acceptor; Q_B, second quinone electron acceptor; RC, reaction center; Chl *a*, chlorophyll *a*; Mes, 4-morpholineethanesulfonic acid; PQ-9, plastoquinone-9; EPR, electron paramagnetic resonance; ENDOR, electron nuclear double resonance; TRIPLE, electron nuclear nuclear triple resonance; **G**, *g*-tensor; **A**, hyperfine tensor; hfc, hyperfine coupling constant.

0006-2960/95/0434-8144$09.00/0

formation (Lubitz et al., 1985; Feher et al., 1985).

The removal of the non-heme Fe^{2+} from PS II seems to be more difficult, and only a few reports are known from the literature. Klimov et al. (1980) decoupled or removed the iron and detected the first X-band EPR spectrum of $Q_A^{\bullet-}$ in PS II. Very recently, it has been shown that addition of cyanide to PS II, which ligates to the iron, leads to the formation of low-spin Fe^{2+} (Sanakis et al., 1994). This offers an alternative way to study the electronic structure of the semiquinone radical anions.

In this paper a technique recently developed in our groups (MacMillan et al., 1990) was applied to generate PS II membrane fragments in which the magnetic interaction between $Q_A^{\bullet-}$ and Fe^{2+} is eliminated, probably owing to an extraction of the metal center. So far, attempts to reconstitute other metals (e.g., Zn^{2+}) have not been successful. However, it has to be emphasized that the procedure used to eliminate Fe^{2+} leaves the electron transfer from pheophytin to Q_A virtually unaffected (Bernarding et al., 1994) and is therefore well suited for studying the properties of $Q_A^{\bullet-}$ by EPR and ENDOR spectroscopy. The magnetic resonance data for $Q_A^{\bullet-}$ in PS II are compared with those obtained from the plastoquinone-9 (PQ-9) anion radical in organic solvents. Preliminary EPR and ENDOR data have been published previously (MacMillan et al., 1990).

MATERIALS AND METHODS

Preparation of Iron-Depleted PS II Membrane Fragments. PS II membrane fragments were prepared according to Berthold et al. (1981) with some modifications as described by Völker et al. (1985). Samples were suspended in iron-free buffer A (20 mM Tricine/NaOH, pH 7.4) at a chlorophyll concentration of 0.5 mg/mL and trypsinized in the dark for 15−30 min (1 mg of trypsin/1 mg of Chl). This treatment blocks the reoxidation of $Q_A^{\bullet-}$ by endogenous or exogenous quinones and greatly enhances the susceptibility to electron abstraction by $K_3[Fe(CN)_6]$ (Renger, 1976). Model studies suggest that the cleavage site attacked by trypsin is very close to the contact area that is assumed to protect the non-heme iron center (Trebst, 1991). Therefore, mild trypsin treatment is expected to enhance the susceptibility of this iron to complexation by exogenous chelators. After 1:1 addition of Fe-depleted buffer B (20 mM MES/NaOH, pH 6.5) and centrifugation (40000*g*), the pellet was resuspended in buffer B and centrifuged (40000*g*). The pellet was resuspended in buffer A containing 1,10-phenanthroline (3 mM) and lithium perchlorate (0.5 M) and stored at 2 °C for 120 min before addition of conalbumin (5%). After centrifugation (40000*g*), the pellet was resuspended in a small amount of buffer A, dialyzed for 12 h (2 °C), diluted with additional buffer A, and centrifuged (40000*g*). The pellet was finally suspended in 500 μL of buffer B and used for EPR measurements. For H/D-exchange experiments the Fe-depleted BBY preparations were freeze-dried. Two portions were resuspended in H_2O and D_2O buffers, respectively. After incubation (1 h), they were again freeze-dried. This procedure was repeated three times.

Characterization of the Iron-Depleted PS II Membrane Fragments. Measurement of the O_2 evolution rate were performed with a conventional Clark type electrode under saturating light intensities and in the presence of phenyl-*p*-benzoquinone and $K_3[Fe(CN)_6]$ as artificial electron acceptors. The activity of the untreated PS II membrane fragments was 300−500 μmol of O_2 per milligram of Chl per hour. The relative number of PS II complexes functionally competent in water oxidation to O_2 was determined from measurements of the averaged O_2 yield per flash (Renger, 1972). Values of 220−280 chlorophylls per fully intact PS II were found. In the iron-depleted samples the water-oxidizing complex (WOC) is severely damaged, leading to a complete loss of the oxygen-evolving capacity. Therefore, the activity of these samples was monitored via flash-induced absorption changes at 320 and 830 nm, reflecting the turnover of Q_A and P_{680}, respectively (Weiss & Renger, 1986). The extent of absorption changes at 830 nm induced by repetitive flash excitation revealed that about 50−70% of PS II was able to perform a stable charge separation in the iron-depleted samples. The relaxation of these signals is dominated by a 10 μs kinetics (Napiwotzski, 1990) indicating that the electron transfer from the tyrosine Y_Z to $P_{680}^{\bullet+}$ is not affected compared with that in samples where the WOC is destroyed by conventional treatments like Tris washing (Conjeaud et al., 1979), treatment with NH_2OH (Eckert et al., 1988a), or mild trypsination (Renger et al., 1984). Likewise, measurements of the absorption changes at 320 nm show that the kinetics of Q_A reduction by the preceding acceptor pheophytin ($Pheo^{\bullet-}$) with a typical rate constant of about 300 ps^{-1} (Eckert et al., 1988b) remains virtually unaffected by the iron-depletion treatment (Bernarding et al., 1994). Inductively coupled plasma (ICP) mass spectroscopy measurements were performed to determine the amount of iron present in the samples. The results showed that the iron-depleted samples contained one fewer iron than the control BBY particles (G. Renger, unpublished results). The ratio of the amplitudes of the flash-induced fluorescence transients measured 100 μs after the first and the second actinic pulse, respectively, permits an estimation of the non-heme iron content that is oxidizable in the dark by $K_3[Fe(CN)_6]$ [for a detailed discussion, see Haag et al. (1992)]. Measurements were performed with home-built equipment (Renger et al., 1988). The data obtained with trypsin-treated control and iron-depleted samples reveal that in the former case oxidizable non-heme iron could be detected as Fe^{3+}, while in the latter sample type virtually no oxidized Fe^{3+} was observed. These findings provide additional evidence that the non-heme iron center is either removed or drastically changed in its microenvironment. Recent Moessbauer studies favor the idea that the non-heme iron is removed from the majority of PS II centers (J. Kurreck, A. Garbers, F. Reifarth, F. Parak, and G. Renger, unpublished results). Lyophilization, which was used in the deuterium-exchange experiments, had no significant effect on the activity of the sample.

Generation of $Q_A^{\bullet-}$. The iron-depleted samples were transferred to quartz EPR tubes (707-SQ, Wilmad) and frozen in liquid nitrogen. Generation of $Q_A^{\bullet-}$ was done by two different methods: (i) chemical reduction of Q_A in iron-depleted BBY membrane fragments with typical Chl *a* concentrations of 6−8 mg mL^{-1} by adding an argon-flushed solution of sodium dithionite (5 mM in 200 mM MES/NaOH, pH 6.5) to the sample (ratio 1:10) in the dark followed by immediate freezing in liquid nitrogen or (ii) photochemical reduction of Q_A by illuminating the frozen samples at 77 K for 10 min using a 500-W white light projector. Alternatively, the samples were placed directly in the EPR cavity cooled to 123 K and illuminated. In order to suppress the formation of other oxidized radical species like Chl $a^{\bullet+}$ and

Y_D^{ox} under these experimental conditions (Vass & Styring, 1991), it was necessary to add a mixture of dichlorophenol indophenol (DCIP, 1 mM) and sodium ascorbate (50 mM) as reductant to the sample before freezing in the dark.

Isolation and Characterization of Plastoquinone-9. Plastoquinone-9 (PQ-9) was extracted from spinach thylakoids in dim green light using a 1:1 mixture of acetone and methanol. The pigments were then extracted into a hydrophobic organic phase (heptane), separated by thin-layer chromatography (TLC), and further purifed by HPLC. No single solvent separates plastoquinone-9 cleanly from the other extracted pigments (Barr & Crane, 1971; Lichtenthaler & Prenzel, 1977). Here toluene was used to separate the plastoquinone-9 from the green components (chlorophylls). This procedure did not separate PQ-9 from β-carotene very well. Therefore, high-performance liquid chromatography (HPLC) was subsequently applied for final purification of PQ-9. For HPLC (Knauer, Berlin) a nucleosil $100C_{18}$ column (pore size, 5 μm; 16 × 250 mm) and a 9:1 solvent mixture of methanol and tetrahydrofuran were used. PQ-9 was dried on a vacuum line and then identified and spectroscopically characterized (MS, ^{1}H-NMR, ^{13}C-NMR, UV-vis) (MacMillan, 1993).

Plastoquinone-9 Anion Radical Generation. The PQ-9 anion radical was generated by dissolving the quinone ($\approx 10^{-3}$ M for frozen samples, 5×10^{-4} M for liquid samples) in slightly basic (potassium *tert*-butylate, 10-fold molar excess) anaerobic solutions of either protonated 2-propanol or fully deuterated (d_8) 2-propanol. These solutions were further deoxygenated in the EPR sample capillaries by bubbling with purified oxygen-free argon for a few minutes and then sealed for liquid solution measurements (in sample tubes with o.d. 2.5 mm) or shock frozen in liquid nitrogen for frozen solution measurements (o.d. 4.0 mm).

Instrumentation. X-band EPR spectra were measured on Bruker ER200D-SRC or ESP-300E spectrometers using a standard rectangular Bruker EPR cavity (ER4102T) equipped with a Bruker nitrogen gas flow system (ER4111VT) for temperature control. Q-band EPR spectra were measured on a Bruker ER 200D EPR spectrometer equipped with a Bruker Q-band microwave bridge, a Bruker ER 5103 QTH resonator, and an Oxford CF 935 cryostat. ^{1}H-ENDOR spectra were recorded using a self-built ENDOR extension consisting of a Rhode & Schwarz radio frequency (rf) synthesiser (SMG), an ENI solid-state rf amplifier (A200L), and a self-built TM_{110} ENDOR cavity adapted to an Oxford helium flow cryostat (ESR 910) which has been described previously (Zweygart et al., 1994). For part of the ENDOR measurements a commercial Bruker ENDOR cavity (ENB200) was used in a setup described earlier (Kurreck et al., 1988).

Analysis of Spectra. (A) EPR. The Q-band EPR powder spectra have been analyzed using a self-written simulation and fit program which is based on the work of Rieger (1982) using a modified Levenberg−Marquardt nonlinear least squares model (Press et al., 1988). This simulation routine includes second-order effects and can deal with an arbitrary number of nuclei with non-colinear g and hf tensors.

(B) ENDOR. In liquid solution ENDOR spectra two lines appear for each magnetic nucleus spaced, to first order, symmetrically around the nuclear Larmor frequency, ν_H, and separated by the respective isotropic hyperfine coupling constant (hfc) a (for $\nu_H > a/2$, which is always the case for the quinones investigated here). The ENDOR frequencies are given by (Kurreck et al., 1988)

$$\nu_{ENDOR}^{\pm} = |\nu_H \pm a/2| \quad (1)$$

In the special TRIPLE experiment the respective high- and low-frequency ENDOR transitions ν^+ and ν^- of a set of equivalent nuclei are induced simultaneously by sweeping two radio frequencies (rf) symmetrically about the proton Larmor frequency (ν_H). The resulting spectrum has the appearance of an "ENDOR half spectrum"; the frequency axis gives the deviation from ν_H. Compared with ENDOR, the special TRIPLE experiment has the advantage of increased signal intensities; furthermore, the amplitudes reflect roughly the relative numbers of contributing nuclei (Dinse et al., 1974; Kurreck et al., 1988, and references therein).

The relative signs of hfc values are determined by general TRIPLE resonance experiments (Biehl et al., 1975; Kurreck et al., 1988, and references therein). In this technique, one ENDOR transition of a particular nucleus is additionally pumped with high rf power while the ENDOR spectrum is recorded. The relative signs of the semiquinone hfc values are obtained from the changes of the relative amplitudes of the high- and low-frequency transitions. Since only lines originating from the same paramagnetic species are affected, this technique can also be used to distinguish between ENDOR lines resulting from different species.

In frozen solutions powder ENDOR spectra are obtained when the magnetic field value is set to the center of the EPR spectrum. For axially symmetric hf tensors with small anisotropy (e.g., methyl group protons) usually both principal values, $A_{||}$ and $A_{\perp}$, can easily be obtained. In the case of a purely dipolar hf tensor, e.g., a hydrogen bond proton, the length of the respective hydrogen bond is estimated using the simple point-dipole approximation (Feher et al., 1985; O'Malley et al., 1985),

$$A(\theta) = \frac{c}{r^3}\varrho(3\cos^2\theta - 1) \quad (2)$$

where $A(\theta)$ is the hyperfine coupling expressed in MHz; $c = g_e\beta_e g_H\beta_H/\hbar$, with g_e and g_H being the electron and proton g-values and β_e and β_H the respective magnetons; ϱ is the unpaired electron spin density at the contact position; θ is the angle between the applied field and the direction of the O−H bond; and r is the magnitude of the O−H distance vector (Å). For randomly oriented molecules one obtains pronounced features in the ENDOR spectrum corresponding to the inflection points of the absorption spectrum which belong to orientations with $\theta = 0°$ and $\theta = 90°$. The signals have characteristic line shapes (Feher et al., 1985, Figure 3), and the hf tensor principal components are related to each other by $A_{||} = -2A_{\perp}$.

At the outer wings of the PQ-9$^{\bullet-}$ EPR spectrum mainly g_{XX} and g_{ZZ} components contribute to the low-field and high-field spectral intensities, respectively. ENDOR spectra recorded at these positions gather mainly intensity from these corresponding molecular orientations (g_{XX} or g_{ZZ}) with respect to the magnetic field axis. This phenomenon has been termed "orientational selection" in ENDOR (Rist & Hyde, 1970). This technique is used to unravel overlapping

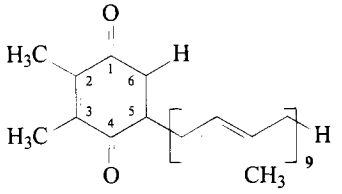

FIGURE 1: Structural formula and numbering scheme of plastoquinone-9 (PQ-9, 2,3-dimethyl-5-solanesyl-1,4-benzoquinone). The proton bound directly to the π-system is called the α-proton (position 6). Protons which are two bonds away from the π-system are called β-protons, e.g., CH_2, position 5, and also CH_3, positions 2 and 3. Protons which are three bonds away from the π-system are called γ-protons, e.g., the proton at the second carbon atom (CH) of the isoprenyl chain at position 5.

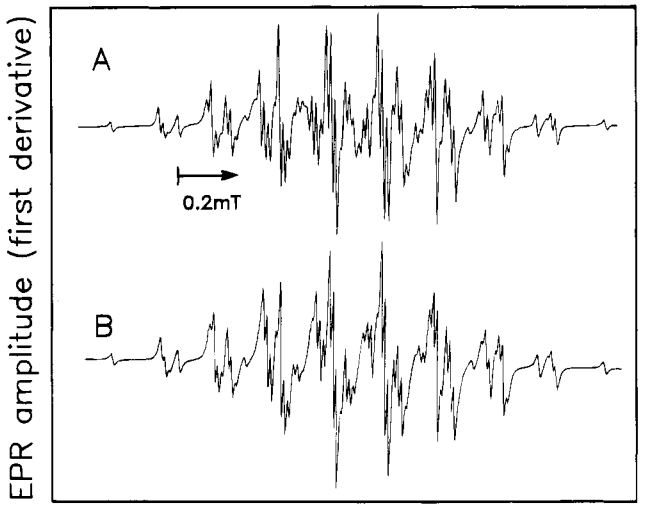

FIGURE 2: Liquid solution EPR spectra of PQ-9$^{\bullet-}$: experiment in protonated 2-propanol at 263 K (A) and simulation (B). The EPR spectrum was simulated using the isotropic proton hfc values from the ENDOR spectrum (see Table 1). The agreement between the simulated and observed EPR spectra proves the correct magnitudes and multiplicities of the measured hfc values. Experimental conditions: microwave power (P_{MW}), 0.2 mW; field modulation depth, 5×10^{-3} mT; accumulation time, 1 min; $T = 263$ K.

$A_{||}$ and $A_{\perp}$ components from different hf tensors of PQ-9$^{\bullet-}$ (see below).

RESULTS AND DISCUSSION

Plastoquinone-9 Anion Radical in Organic Solvents

Liquid Solution Spectra. For an interpretation of the EPR and ENDOR results obtained from $Q_A^{\bullet-}$ in iron-depleted PS II membrane fragments an understanding of the electronic structure of the anion radical of the isolated PQ-9 (Figure 1) in organic solvents is indispensable. In liquid solutions anisotropic hyperfine interactions are averaged out, and a well-resolved EPR spectrum of this species can be obtained, which is shown in Figure 2A together with a simulation (Figure 2B) using the hfc values of Table 1.

The ^{1}H-ENDOR spectrum of PQ-9$^{\bullet-}$ obtained in liquid solution is depicted in Figure 3C. Four line pairs spaced symmetrically about the free proton frequency are clearly resolved, yielding four isotropic hfc values which are assigned to the protons of the four substituents at the quinone ring (Table 1). A much smaller hfc, assigned to the γ-proton of the isoprenyl chain, is detected under high-resolution conditions (Figure 3C, inset). The assignment of the four large hfc values to individual protons at ring positions 2, 3, 5, and 6 (Figure 1) is achieved by using additional techniques such as special and general TRIPLE resonance and by investigating the temperature dependence of the observed

Table 1: Isotropic Hyperfine Coupling Constants of the PQ-9 Radical Anion (MHz)

molecular position[a]					
2 -CH_3	3 -CH_3	5 -CH_2	6 α-H	5 γ-H	ref
+4.943	+5.322	+6.870	−5.740	±0.306	*b*
+4.75	+5.72	+6.99			*c*
4.99	5.30	6.70	5.72		*d*
5.0	5.0	6.7	5.6		*e*

[a] For molecular positions, see Figure 1. [b] This work: ENDOR, solvent, 2-propanol at $T = 263$ K; error, ±0.005 MHz; signs determined by general TRIPLE resonance. [c] This work: ENDOR, solvent, 2-propanol at $T = 223$ K; error, ±0.01 MHz. [d] EPR in ethanol at ambient temperature (Kohl et al., 1969). [e] EPR in ethanol at ambient temperature (Pedersen, 1978).

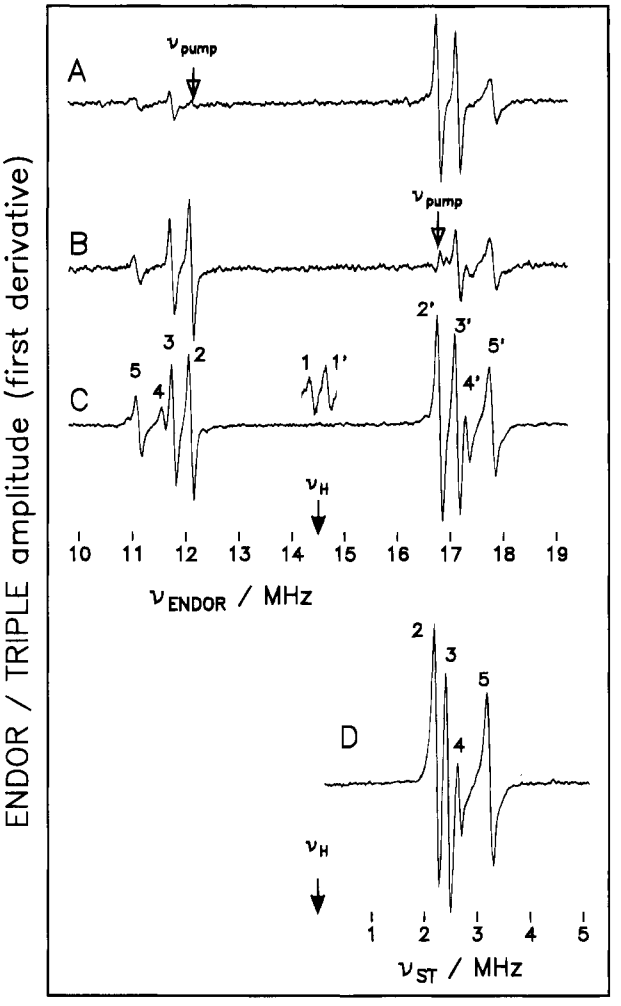

FIGURE 3: Liquid solution ^{1}H-ENDOR (C), general TRIPLE (A and B), and special TRIPLE (D) spectra of PQ-9$^{\bullet-}$ in protonated 2-propanol. In the special TRIPLE experiment the frequencies for the line positions correspond to one-half of the respective hfc. Corresponding high- and low-frequency lines are numbered (C), and the respective hfc values are given in Table 1. Experimental conditions: (C) ENDOR spectrum, P_{MW}, 8 mW; radio frequency power (P_{RF}), 50 W; frequency modulation (FM), 12.5 kHz; FM depth (ΔFM), 50 kHz; accumulation time, 8 min; $T = 263$ K (inset at $T = 293$ K). (A and B) General TRIPLE, P_{MW}, 8 mW; P_{RF}, 50 W (scan), 50 W (sweep); FM, 12.5 kHz; ΔFM, 50 kHz; accumulation time, 30 min; $T = 263$ K. (D) Special TRIPLE, P_{MW}, 8 mW; P_{RF}, 2 × 50 W; FM, 12.5 kHz; ΔFM, 50 kHz; accumulation time, 30 min; $T = 293$ K.

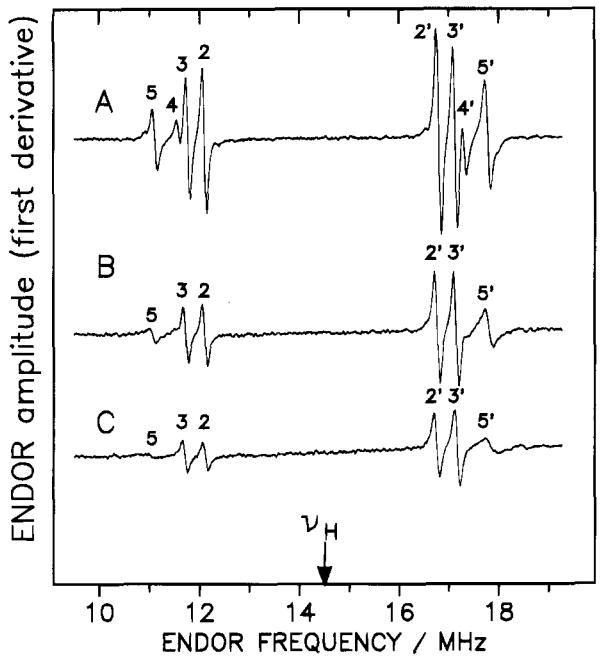

FIGURE 4: ENDOR spectra of PQ-9$^{\bullet-}$ obtained at different temperatures in protonated 2-propanol: 263 (A), 233 (B), and 203 K (C). For other experimental conditions, see Figure 3.

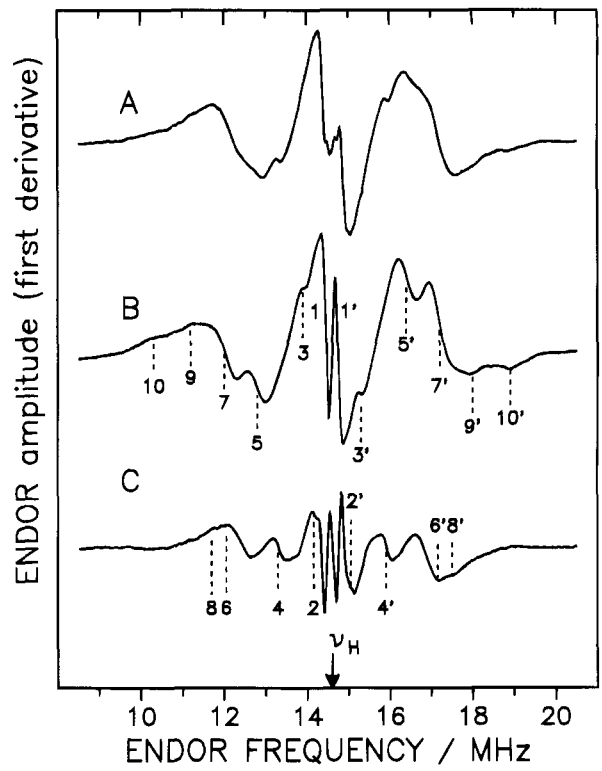

FIGURE 5: Frozen solution ^{1}H-ENDOR spectra of PQ-9$^{\bullet-}$ in protonated (A) and fully deuterated (B) 2-propanol and their difference (A − B) spectrum (C). Experimental conditions: P_{MW}, 8 mW; P_{RF}, 100 W; FM, 12.5 kHz; ΔFM, 50 kHz; accumulation time, 10 min; T = 123 K. Corresponding high- and low-frequency lines from which the hf splittings are obtained (Table 2) are numbered in the spectra (B, C).

hfc values. The special TRIPLE spectrum of PQ-9$^{\bullet-}$, where signal amplitudes reflect approximately the number of contributing protons, is depicted in Figure 3D. The line amplitude ratio of 3:3:1:2 immediately allows a specific assignment to methyl, methyl (positions 2 and 3), α-proton (position 6), and methylene groups (position 5), respectively (see Figure 1).

The α-proton couplings can also be discriminated from those of the methylene and methyl proton couplings on the basis of the different signs of the corresponding hfc values. For positive π-spin densities at the adjacent carbon atom α-protons have negative hfc values, whereas β-protons (like methylene and methyl) have positive hfc values (Carrington & McLachlan, 1967). The general TRIPLE spectra of PQ-9$^{\bullet-}$ (Figure 3A,B) confirm that the hyperfine coupling belonging to the line pair 4,4′ has a different (negative) sign with regard to the methyl and methylene proton hyperfine couplings, which are positive (Table 1).

Additional information is obtained using the temperature dependence of the hyperfine couplings (see Figure 4). At 263 K (Figure 4A) four line pairs are clearly visible in the ENDOR spectrum. At lower temperature (233 K, Figure 4B) the intensities of the lines belonging to the α-proton (4,4′) become very weak due to unfavorable relaxation conditions decreasing the ENDOR enhancement. This is a consequence of the larger anisotropy of the α-proton hyperfine coupling as compared with those of the methyl and methylene protons [see Kurreck et al. (1988), chapter 3]. The observed broadening (203 K, Figure 4C) of the line belonging to the methylene protons (5,5′) is due to hindered rotation of the long isoprenoid chain (Das et al., 1970).

Frozen Solution Spectra. In frozen samples ($T \leq$ 150 K) the resonances from each group of protons are smeared out over the complete range of anisotropic hf tensor values (Figure 5A). Due to their small hf anisotropy and near axial symmetry the fairly strong lines of the protons of the freely rotating methyl groups are most easily identified, whereas the lines of the methylene protons are broadened beyond detection. Additional resonances from purely dipolar (matrix) interactions of the surrounding (e.g., hydrogen-bonded) protons are no longer averaged out and contribute to the spectra. The components of the anisotropic hyperfine tensors of different types of protons can, however, be discriminated in these types of spectra using the methods shown in Feher et al. (1985).

Anisotropic HF Interactions of Exchangeable Protons. If fully deuterated alcohol is used as a solvent (Figure 5B), the ENDOR spectrum is altered, indicating that some of the hyperfine couplings observed in protonated medium belong to exchangeable protons. These protons are assigned to surrounding solvent molecules which form hydrogen bonds to the oxygen atoms of the quinone.

In the difference spectrum (Figure 5C) four line pairs appear at positions which are different from those of the features in Figure 5B. Two of these line pairs (6,6′ and 4,4′) are assigned to hf tensor components $|A_{1\|}|$ = 5.1 MHz and $|A_{1\perp}|$ = 2.6 MHz. On the basis of their line shapes and the ratio of their hf values they are assigned to the parallel and perpendicular components of an essentially traceless axially symmetric tensor of a hydrogen-bonded proton ($A_{\|} > 0$; $A_{\perp} < 0$). These values are typical for the hydrogen bond protons of quinone anion radicals lacking bulky substituents and are very similar to the values observed for the 1,4-benzoquinone anion radical (O'Malley et al., 1985; MacMillan, 1993). Using the point-dipole approximation (eq 2) and an oxygen π-spin density (ϱ_o^{π}) of 0.22, which is an average value for several different quinone anion radicals in different environments obtained from ^{17}O-EPR measurements (Lubitz et al.,

1985; Feher et al., 1985), a hydrogen bond distance of $r_{O-H} \approx 1.9$ Å is obtained from the tensor $\mathbf{A_1}$.

Two additional features observed in Figure 5C (line pairs 8,8′ and 2,2′) correspond to hf tensor components $|A_{2||}| = 5.8$ MHz and $|A_{2\perp}| = 0.85$ MHz; they are also assigned to exchangeable protons. The interpretation of this second hf tensor is more difficult. Assuming that $A_{2||} = (+)5.8$ MHz and $A_{2\perp} = (-)0.85$ MHz, it has an isotropic part of $\frac{1}{3}\mathrm{Tr}_{A_2} \approx 1.4$ MHz. If $A_{2\perp}$ were positive, a much larger A_{iso} of 2.5 MHz would be obtained, which is unlikely. The isotropic part of the hf coupling is rationalized by the fact that the hydrogen bond is no longer in the plane of the molecule but rather approaches the oxygen atom from above (or below) the molecular plane due to the bulky ring substituents. Similar hyperfine couplings from exchangeable protons have been found in the frozen solution ENDOR spectra of the tetramethyl-1,4-benzoquinone anion radical and several other related radicals where bulky substituents prevent the formation of H-bonds in the molecular plane (MacMillan, 1993). The isotropic part, A_{iso} (≈1.4 MHz), probably results from direct orbital overlap with the oxygen π-orbital. The purely dipolar tensor then has components $A'_{2||} = 4.4$ MHz and $A'_{2\perp} = -2.25$ MHz. Using eq 2 and a ϱ_O^π of 0.22 leads to a hydrogen bond length of $r_{O-H} \sim 2.0$ Å. The two different H-bond tensors, $\mathbf{A_1}$ and $\mathbf{A_2}$, observed here strongly suggest that two dominant H-bonds of different strengths and geometries exist to the two carbonyl oxygens of $PQ\text{-}9^{\bullet-}$ in frozen alcoholic solutions. Since tensor $\mathbf{A_1}$ is essentially traceless ($A_{iso} \approx 0$), the corresponding stronger H-bond is expected to lie in the molecular plane of PQ-9. This is similar to the hydrogen bonds found for the unsubstituted benzoquinone anion radical (O'Malley & Babcock, 1986; Burghaus et al., 1993; MacMillan, 1993). On the basis of steric arguments tensor $\mathbf{A_1}$ is assigned to O_1, whereas the tensor $\mathbf{A_2}$ (and the corresponding weaker hydrogen bond) is assgined to O_4. The pair of narrow lines in the center of the spectrum shown in Figure 5C close to the matrix region can be assigned to an additional, very weak hydrogen bond interaction with an estimated length of approximately 3 Å. Similar weak hydrogen bonds have also been detected by O'Malley & Babcock (1986) for the 1,4-benzoquinone anion radical and other simple quinone anion radicals (MacMillan, 1993).

Anisotropic HF Interactions of the CH_3-, CH_2-, and α-Protons. The best spectral resolution for the protons belonging to $PQ\text{-}9^{\bullet-}$ is obtained from samples measured in deuterated medium (Figure 5B). In frozen solution only protons of rotating methyl groups give rise to narrow and intense ENDOR lines (Hyde et al., 1968). Lines from α-protons and from fixed β-protons (CH_2 groups) are broadened and not easily detected. From Figure 5B two different nearly axially symmetric methyl hyperfine tensors can be determined with the help of orientation-selected ENDOR experiments (Rohrer et al., 1995) performed at different positions on the EPR spectrum [data not shown; see MacMillan (1993)]. Since the isotropic methyl hfc values are positive, it follows that the $A_{||}$ and $A_\perp$ values are all positive. The obtained methyl group tensor components are given in Table 2.

Orientation-selected ENDOR experiments also revealed two of the three components of the α-proton hyperfine tensor in deuterated 2-propanol ($A_{XX} = -9.0$ MHz, and $A_{ZZ} = -8.0$ MHz; spectra not shown). Assuming the same isotropic hfc value as observed in liquid solution ($A_{iso} = -5.74$ MHz), the third component is expected to be $A_{YY} = -0.22$ MHz. The corresponding ENDOR splitting could therefore belong to one of the features 1,1′ or 3,3′ (Figure 5B). The observed hyperfine tensor is nearly axially symmetric, which is unusual for α-protons. A similar α-proton hf tensor has, however, been found in 1,4-benzoquinone using X-band ENDOR (O'Malley & Babcock, 1986; MacMillan, 1993) and W-band EPR experiments (Burghaus, 1991; Burghaus et al., 1993). These tensor values have been rationalized by the presence of the large spin densities on the adjacent carbonyl groups.

Table 2: Hyperfine Splittings (MHz) for $PQ\text{-}9^{\bullet-}$ in Frozen Solution of Deuterated and Protonated 2-Isopropanol

line pairs	type of proton[a]	$\mathbf{A}_{||}$[b]	$\mathbf{A}_\perp$[b]	1/3Tr $\mathbf{A}$[b]	$\frac{A_{||} - A_\perp}{A_{iso}}$[c]	molecular position
10,10′	CH_3	(+)8.58				3
7,7′			(+)5.29			
				(+)6.39	0.51	
9,9′	CH_3	(+)6.68				2
5,5′			(+)3.70			
				(+)4.69	0.64	
6,6′	H-bond	(+)5.10				to O_1
4,4′			(−)2.60			
				−0.03		
8,8′	H-bond	(+)5.80				to O_4
2,2′			(−)0.85			
				+1.37		

[a] The α-proton tensor is discussed in the text. [b] Error, ±0.05 MHz. The signs have not been obtained directly (see text). [c] Measure of anisotropy.

Unlike the methyl protons, the methylene protons in the isoprenoid chain are not expected to rotate freely. The chain might be locked in several conformations leading to a spread of values for the dihedral angles which determine the magnitude of the β-proton (CH_2) hfc values (Carrington & McLachlan, 1967). Therefore, in frozen solution at 123 K, the methylene proton lines could not be detected in our ENDOR experiments.

Temperature Dependence of the Hyperfine Couplings. Additional evidence for the asymmetric hydrogen bonding is provided by the temperature dependence of the four large hyperfine couplings (Figure 4). The isotropic hyperfine couplings from the protons of the two ring methyl groups are already inequivalent at room temperature due to the asymmetric substitution pattern of the PQ-9 molecule. When the temperature is lowered, the difference between the hfc values increases. Inspection of the proton hfc values in Table 1 shows that one methyl proton hfc and the methylene proton hfc (position 5) increase, whereas the hfc of the second methyl group decreases. These shifts may be explained by a change of the spin density within the molecule caused by a larger difference of the relative strengths of the two hydrogen bonds to the quinone oxygens. As depicted in the valence bond structures (Scheme 1), the shift in spin density caused by the formation of a strong hydrogen bond to the oxygen at C_1 causes an increase of spin density at positions 1, 3, and 5 and a concomitant reduction at positions 2, 4, and 6. In the limiting case of a neutral semiquinone radical protonated at oxygen O_1 the spin densities at positions 3 and 5 have been shown experimentally to be about twice as large as in the anion radical, whereas those at positions 2 and 6

Scheme 1

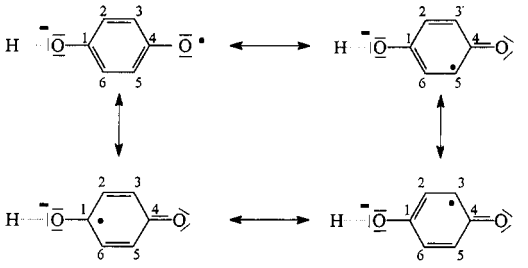

are very small and even change sign (Pederson et al., 1975). Since the stronger hydrogen bond has been assigned to O_1 in PQ-9$^{\bullet-}$, the larger methyl proton tensor is assigned to position 3. The temperature dependence of the hyperfine couplings shows that in PQ-9$^{\bullet-}$ the strength of the H-bond to O_1 increases at lower temperatures as compared to that of the H-bond to O_4.

The shifts of spin density between positions 3,5 and 2,6 which are predicted from Scheme 1 are qualitatively reproduced in MO calculations using RHF-INDO/SP (Plato et al., 1991). The hydrogen bonds to the quinone oxygens were simulated by point charges near the oxygens. The calculations showed that the charges must be placed at different distances (e.g., 1.6 Å to O_1 and 2.0 Å to O_4) and orientations to the quinone oxygens, with the point charge at O_1 being in the plane and closer than the point charge at O_4, which is twisted out of the plane in order to obtain a satisfying agreement with the experimental hfc values (MacMillan, 1993).

In summary, for PQ-9$^{\bullet-}$ a complete set of isotropic hyperfine couplings could be determined by ENDOR and TRIPLE resonance in liquid solution. In the frozen state the hf tensor values for both methyl groups and the α-proton were obtained, whereas no hyperfine couplings could be observed from the protons of the isoprenoid chain probably due to conformational disorder. Magnitudes and temperature dependences of the hyperfine couplings on PQ-9$^{\bullet-}$ indicate an asymmetric interaction of the quinone oxygens with the solvent matrix. A direct detection of two hydrogen bonds of different strengths and geometries and an additional weak one became possible by analysis of the respective proton hf tensors. These results form the basis for an analysis of the $Q_A^{\bullet-}$ spectra in PS II.

$Q_A^{\bullet-}$ in PS II Membrane Fragments

X-Band (9 GHz) EPR of $Q_A^{\bullet-}$ in PS II Membrane Fragments. In PS II membrane fragments the semiquinone radical anion $Q_A^{\bullet-}$ coupled to the high-spin Fe^{2+} exhibits an EPR signal ($Fe^{\bullet 2+}$ $Q_A^{\bullet-}$) which can be observed only at very low temperatures (Nugent et al., 1981). The g-value of this signal depends on pH with $g = 1.82$ at pH < 7.0 and $g = 1.9$ at higher pH (Rutherford & Zimmermann, 1984). This signal with $g = 1.82$ in PS II is very similar to the signal of the semiquinone anion interacting with the iron in purple bacteria (Feher & Okamura, 1978). It was found that this EPR signal in PS II is affected by herbicide binding (Atkinson & Evans, 1983; Rutherford et al., 1984). Likewise, replacement of HCO_3^- by formate greatly enhances the signal amplitude (Vermaas & Rutherford, 1984; Bowden et al., 1991).

Here this signal is used to verify that in the iron-depleted samples the Fe^{2+} is either removed or at least decoupled from

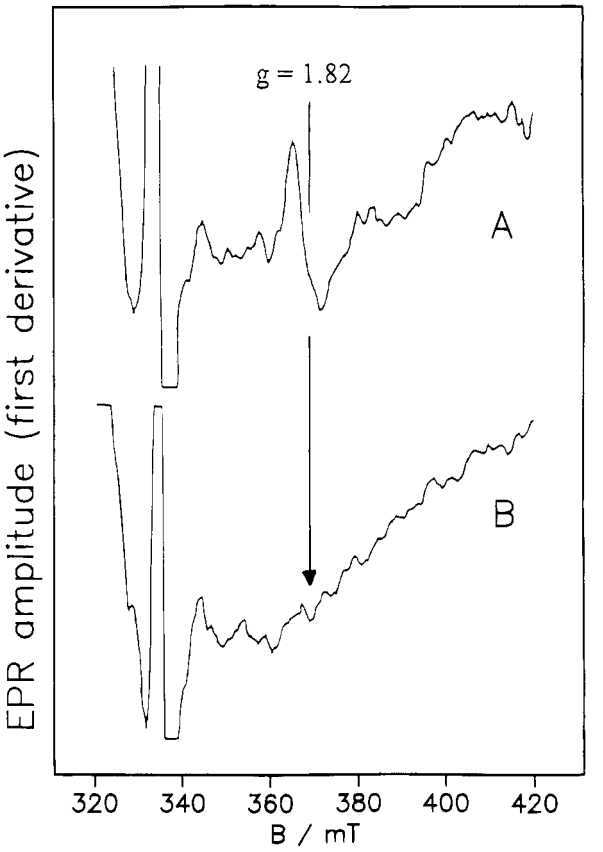

FIGURE 6: EPR signal from the $Fe^{2+}Q_A^{\bullet-}$ complex in illuminated PS II membrane fragments (A) and EPR spectrum of the respective iron-depleted sample (B). Note that in (B) no $Fe^{2+}Q_A^{\bullet-}$ complex signal at $g = 1.82$ is detected. Experimental conditions: P_{MW}, 20 mW; microwave frequency, 9.5 GHz; field modulation depth, 1.6 mT, frequency, 100 kHz; accumulation time, 200 s; $T = 2$ K; sample concentrations, 10 mg of Chl *a* mL^{-1} (A) and 13 mg of Chl *a* mL^{-1} (B).

$Q_A^{\bullet-}$. The technique of signal enhancement by formate has been applied for measurements in all samples. A typical trace of an untreated PS II membrane fragment control sample is shown in Figure 6A. A similar spectrum is also detected in trypsin-treated samples (data not shown), indicating that this treatment does not markedly affect the iron–quinone interaction in these preparations. Similar conclusions were drawn previously (Renger et al., 1985). In contrast, this signal is no longer detected in the iron-depleted samples (Figure 6B), showing that the iron is either removed or at least magnetically decoupled from the $Q_A^{\bullet-}$.

At the same time a new narrow EPR signal at $g = 2.0048$ is detected when the samples are illuminated in the presence of DCIP and sodium ascorbate (Figure 7C). This signal could also be generated by chemical reduction in the dark with an excess of sodium dithionite (Figure 7A). Only the iron-depleted sample gave this EPR signal. This result unambiguously shows that the electron acceptor radical anion $Q_A^{\bullet-}$ decoupled from the magnetic interaction with the nonheme iron can be generated chemically *and* photochemically in the iron-depleted preparations. Both the g-factor and the line width (Table 3) are very similar to values observed for the immobilized PQ-9$^{\bullet-}$ in organic solvents (Figure 7B). Signals with similar g-values have been observed in other types of membrane fragments (Klimov et al., 1980) and also in PS II core complexes (Adir et al., 1992). More recently in cyanide-treated BBY membrane fragments (Sanakis et al.,

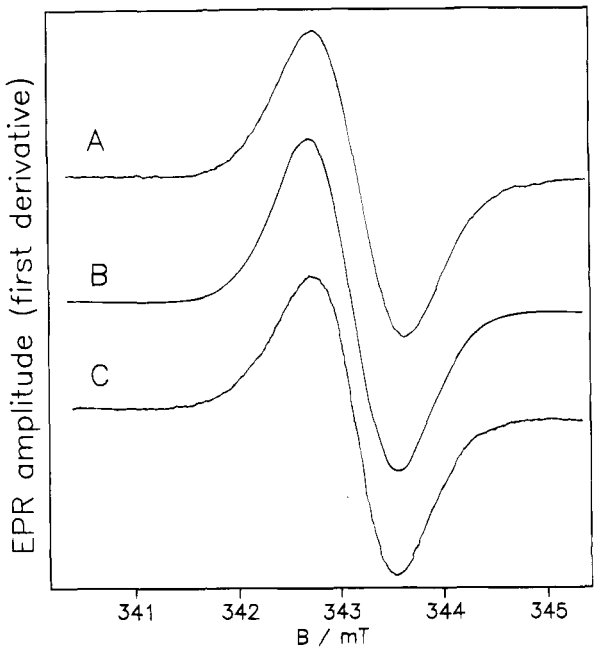

FIGURE 7: EPR spectra of iron-depleted membrane fragment samples: Dark-adapted samples treated with dithionite (A; for details, see text), PQ-9$^{\bullet-}$ in alkaline protonated 2-propanol (B), and iron-depleted sample after illumination in the presence of DCIP and ascorbate at 77 K for 10 min (C). Experimental conditions: P_{MW}, 2 mW; field modulation depth, 0.2 mT; accumulation time, 40 s; T = 123 K; concentrations of samples, 8 mg of Chl a mL^{-1} (A, C) and 10^{-3} M (B).

1994) a very similar signal was described and has been assigned to the plastosemiquinone anion radical, $Q_A^{\bullet-}$.

In order to verify this assignment, the control PS II samples and each of the successive steps in the treatment were characterized using EPR spectroscopy. The results obtained are summarized in Table 3. Dark-adapted control PS II samples show the typical EPR signal II_s belonging to oxidized tyrosine Y_D^{ox}. When these samples are treated with trypsin, signal II_s is no longer detected. This observation agrees with earlier EPR studies on the modification of the PS II donor side induced by trypsinization at pH = 7.5 (Völker et al., 1986). Upon illumination signal II_S does not reappear, but a new EPR signal is observed at g = 2.0028 having a line width of 0.89 mT. This signal is assigned to a monomeric chlorophyll a cation radical. Recently two different Chl a cation radicals in PS II have been characterized together with $P_{680}^{\bullet+}$ by ENDOR (Rigby et al., 1994). Our hfc values obtained for this species by ENDOR (MacMillan, 1993) are given in Table 3 (caption) and agree well with those from Chl $a^{\bullet+}$ (I) in Rigby et al. (1994) and with those of Chl $a^{\bullet+}$ in organic solvents (Käss et al., 1994).

Further treatment of the samples with 1,10-phenanthroline and lithium perchlorate to remove the high-spin iron leads to a slight shift in the g-value of this light-induced EPR signal toward higher values. The spectrum now appears to contain two overlapping EPR signals (data not shown). If these samples are illuminated in the presence of DCIP and sodium ascorbate, an EPR signal at g = 2.0048 with a line width of 1.01 mT is detected which is very similar to that of PQ-9$^-$ (Figure 7B,C). This demonstrates, in agreement with the measured absorption changes at 320 nm, that electron transfer from pheophytin to Q_A is still functioning in these iron-depleted samples. In order to avoid any contributions of photoinduced Chl $a^{\bullet+}$ or Y_D^{ox} due to incomplete reduction, the ENDOR experiments were performed on samples where $Q_A^{\bullet-}$ was generated with dithionite in the dark (Figure 7A; Table 3).

H_2O/D_2O-exchange experiments were performed to detect exchangeable protons belonging to possible hydrogen bonds to the quinone oxygens and thereby characterize the Q_A binding site in the protein matrix. A significant narrowing of the $Q_A^{\bullet-}$ EPR signal is observed in the D_2O-exchanged samples [the first-derivative EPR peak to peak line width (ΔB_{pp}) reduces from 0.98 to 0.87 mT], indicating the presence of large hyperfine couplings from these exchangeable protons. The observed effect is of comparable magnitude to that observed for PQ-9$^{\bullet-}$ in frozen protonated and deuterated 2-propanol. The characteristic parameters of the EPR signals and their assignments to different radicals in these samples are given in Table 3.

^{1}H-ENDOR of $Q_A^{\bullet-}$ in PS II Membrane Fragments. The ENDOR spectra of $Q_A^{\bullet-}$ in H_2O- and D_2O-exchanged iron-depleted samples generated by reduction in the dark with sodium dithionite are shown as spectra A and B, respectively, in Figure 8. Identical ENDOR spectra of the samples in H_2O were observed before and after the lyophilization. The spectrum measured in D_2O is better resolved due to the absence of hyperfine couplings from exchangeable protons; six hyperfine components (see line pairs in Figure 8B) are clearly resolved. This spectrum is difficult to interpret, as it is only observed in frozen solution and no additional information about the isotropic hyperfine couplings—as for PQ-9$^{\bullet-}$—is available. The major problem is the correct assignment of the observed hf components to specific protons in $Q_A^{\bullet-}$.

Methyl Proton hf-Tensors. The hyperfine tensors of the two methyl groups at positions 2 and 3 (Figure 1) are assigned in analogy to PQ-9$^{\bullet-}$ and to the results obtained for a series of other quinone anion radicals (MacMillan, 1993) and for $Q_A^{\bullet-}$ and $Q_B^{\bullet-}$ in bacterial reaction centers (Feher et al., 1985). The presence of large π spin densities at the carbonyl carbon and oxygen atoms leads to modified hyperfine tensors for the methyl groups attached to the quinone ring. Each carbonyl group carries approximately 40% of the π-spin density (summed over the carbon and oxygen atoms), whereas only ca. 5% is found at each ring carbon (positions 2, 3, 5, and 6, Figure 1). Therefore, these methyl proton hf tensors exhibit large hyperfine anisotropies. Normally the methyl proton hyperfine anisotropy is very small ($\approx$0.2) when neighboring spin densities are comparable or even smaller than that of the ring π-carbon adjacent to the methyl group. The hyperfine anisotropies of the methyl groups attached to the quinone ring, defined as

$$\frac{A_{\parallel} - A_{\perp}}{A_{iso}} \qquad (3)$$

are 0.51 and 0.64 for PQ-9$^{\bullet-}$ in 2-propanol (Table 2) and remain fairly constant for a series of substituted semiquinone anion radicals (MacMillan, 1993) and also for $Q_A^{\bullet-}$ and $Q_B^{\bullet-}$ in bacterial reaction centers (Feher et al., 1985). For $Q_A^{\bullet-}$ in *Rhodobacter sphaeroides* recently a value of 0.71 has been determined with high accuracy from ENDOR experiments on reaction center single crystals (Isaacson et al., 1995a). Furthermore, it has been found that the sum of the π-spin densities at positions 2, 3, 5, and 6 (and therefore also the

Table 3: *g*-Factors and EPR Line Widths (ΔB_{pp}) of Differently Treated PS II Membrane Fragments

sample[a]	dark		light		signal assignment	ref
	g-factor[b]	ΔB_{pp} (mT)	*g*-factor[b]	ΔB_{pp} (mT)		
BBY	2.0052	1.60	2.0052	1.60	Y_D^{ox} + Chl $a^{\bullet+}$	*c*
BBY + trypsin			2.0028	0.89	Chl $a^{\bullet+}$ [f]	*c*
BBY + trypsin + O-Phen/$LiClO_4$			2.0030	0.88	Chl $a^{\bullet+}$ + $Q_A^{\bullet-}$	*c*
BBY + trypsin + O-Phen/$LiClO_4$ + DCIP/Asc			2.0048	1.01	$Q_A^{\bullet-}$	*c*
BBY + $S_2O_4^{2-}$	2.0049	1.60	2.0049	1.60	Y_D^{ox}	*c*
BBY + trypsin + $S_2O_4^{2-}$			2.0030	0.89	Chl $a^{\bullet+}$	*c*
BBY + trypsin + O-Phen/$LiClO_4$ + $S_2O_4^{2-}$	2.0049	1.00	2.0049	1.00	$Q_A^{\bullet-}$	*c*
BBY + trypsin + O-Phen/$LiClO_4$ + H_2O ex + $S_2O_4^{2-}$	2.0049	0.98	2.0049	0.98	$Q_A^{\bullet-}$	*c*
BBY + trypsin + O-Phen/$LiClO_4$ + D_2O ex + $S_2O_4^{2-}$	2.0048	0.87	2.0048	0.87	$Q_A^{\bullet-}$	*c*
PQ-$9^{\bullet-}$ in protonated 2-propanol	2.00457	0.987			PQ-$9^{\bullet-}$	*d*
PQ-$9^{\bullet-}$ in fully deuterated 2-propanol	2.00465	0.825			PQ-$9^{\bullet-}$	*d*
Chl $a^{\bullet+}$ in CH_2Cl_2/THF	2.0025	0.79−0.95			Chl $a^{\bullet+}$	*e*

[a] O-Phen = 1,10-phenanthroline; DCIP = dichlorophenol indophenol; Asc = sodium ascorbate; THF = tetrahydrofuran. [b] All *g*-factors are corrected (against phenalenyl, g = 2.00262) error, ±0.0001. [c] This work. [d] MacMillan, 1993. [e] Lubitz, 1991. [f] Methyl hf tensor components and assignments (positions in brackets) for Chl $a^{\bullet+}$: 3.0 MHz (*2*), 3.6 MHz (*7*), and 7.2 MHz (*12*); see Käss et al. (1994) for numbering.

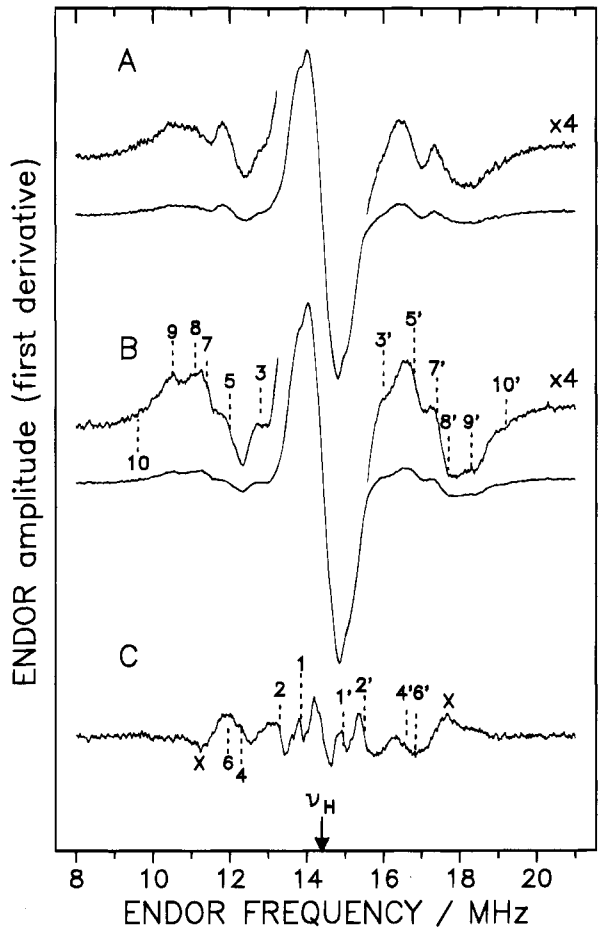

FIGURE 8: ^{1}H-ENDOR spectra of $Q_A^{\bullet-}$ in iron-depleted PS II membrane fragment samples in H_2O buffer (A) and D_2O buffer (B) and their difference (C, A − B; the features labeled X are subtraction artifacts). The samples (concn: 6 mg of Chl mL^{-1}) were reduced chemically with sodium dithionite (see text). Experimental conditions: P_{MW}, 6 mW; P_{RF}, 100 W; FM, 12.5 kHz; ΔFM, 200 kHz; accumulation time, 120 min each; T = 20 K. Corresponding high- and low-frequency lines from which the hf splittings are obtained (Table 4) are numbered in the spectra (B, C).

sum of the proton hfc values of attached methyl groups) stays fairly constant in a series of different quinone anion radicals (MacMillan, 1993). Hydrogen bonds to the carbonyl oxygens mainly cause shifts of π-spin densities (see Scheme 1); e.g., for a H-bond to O_1, shifts from O_1 to C_1, from C_4 to O_4, from C_2 to C_3, and from C_6 to C_5 occur with concomitant

Table 4: Hyperfine Splittings (MHz) from $Q_A^{\bullet-}$ in Frozen Solution in Deuterated and Protonated Buffer

line pairs[a]	type of proton	$A_{\parallel}$[b]	$A_{\perp}$[b]	1/3Tr **A**[b]	$\frac{A_{\parallel} - A_{\perp}}{A_{iso}}$	molecular position
9,9′	CH_3	(+)7.8				3
5,5′			(+)4.8			
				(+)5.8	0.52	
8,8′	CH_3	(+)6.7				2
3,3′			(+)3.3			
				(+)4.4	0.77	
4,4′	H-bond	(+)4.4				to O_1
2,2′			(−)2.2			
				0.0		
6,6′	H-bond	(+)4.8				to O_4
1,1′			(−)1.1			
				+0.9		

[a] For a discussion of transitions 7,7′ and 10,10′ and signs of hfc values, see text. [b] Errors, ±0.1 MHz.

changes of the attached isotropic methyl proton hfc values, which are directly proportional to the π-spin density at the adjacent π-carbon atom.

On the basis of conserved hyperfine anisotropy and conserved sum of the isotropic hfc values of the methyl hf tensors in PQ-$9^{\bullet-}$ and $Q_A^{\bullet-}$ we assign the line pairs 3,3′ and 5,5′ to the perpendicular components [$A_{\perp}(2)$ and $A_{\perp}(3)$] of the methyl hf tensors at positions 2 and 3. This is confirmed by orientation-selected ENDOR measurements (data not shown). The shoulders 8,8′ and 9,9′ (peaks in the first-derivative spectrum) are assigned to the respective $A_{\parallel}$ components. The sum of the isotropic part of the two methyl proton hf tensors is then 10.2 MHz; the corresponding value for PQ-$9^{\bullet-}$ is 11.1 MHz. The anisotropy (eq 3) is 0.77 for the methyl group at position 2 and 0.52 for position 3 as compared with 0.64 and 0.51 for the respective values in PQ-$9^{\bullet-}$ (Table 2). The difference in the isotropic parts, A_{iso} (5.8 and 4.4 MHz), indicates an asymmetrical hydrogen-bonding situation. We assign the large hfc to position 3 on the basis of the assumption that the hydrogen bond to O_1 is stronger than the hydrogen bond to O_4 (see above discussion for PQ-$9^{\bullet-}$). The relative shifts of the hyperfine couplings at positions 2 and 3 induced by different hydrogen bonds to oxygens O_1 and O_4 are also predicted by MO calculations (see above). The hf tensor components for the methyl groups are given in Table 4.

Hydrogen Bond Protons. The hyperfine couplings of the hydrogen bond protons have also been elucidated. The difference of the spectra measured in protonated and deuterated buffer (Figure 8C) is similar to the difference spectrum found for PQ-9$^{\bullet-}$ in frozen alcohol. The line pairs 2,2′ and 4,4′ with corresponding hyperfine components of 2.2 and 4.4 MHz are interpreted as $A_\perp$ and $A_\parallel$ components of a purely dipolar hyperfine coupling of a hydrogen bond proton as has been observed for the stronger hydrogen bond in PQ-9$^{\bullet-}$ and in other semiquinone anion radicals (MacMillan, 1993). Using eq 2 and an oxygen π-spin density of 0.22, a hydrogen bond distance of 2.0 Å is obtained, which is somewhat longer than that for PQ-9$^{\bullet-}$ in frozen alcoholic solution (1.9 Å).

Two additional line pairs, 6,6′ and 1,1′, in the difference spectrum with corresponding hyperfine components of (+)4.8 and (−)1.1 MHz are interpreted in analogy to PQ-9$^{\bullet-}$ as $A_\parallel$ and $A_\perp$ components of a second H-bond. The isotropic part of this hf tensor (+0.9 MHz) indicates that this second hydrogen bond is twisted out of the plane of $Q_A^{\bullet-}$, the dipolar part indicates a similar H-bond length as in PQ-9$^{\bullet-}$ in frozen alcoholic solution. These data show that the hydrogen bond to O_1 is somewhat weaker as compared with PQ-9$^{\bullet-}$ *in vitro*, while the hydrogen bond to O_4 is of similar strength. This is in agreement with the shift of the g_{XX} component of the g tensor observed in the Q-band EPR spectra for $Q_A^{\bullet-}$ as compared with PQ-9$^{\bullet-}$ (see below), which indicates weaker hydrogen bonds for $Q_A^{\bullet-}$ and/or a more aromatic environment.

Methylene and α-Protons. In contrast to PQ-9$^{\bullet-}$ in 2-propanol, the isoprenyl chain in $Q_A^{\bullet-}$ is expected to have a well-defined conformation imposed by the protein matrix, and the lines of the methylene protons may then appear in the ENDOR spectra. Possible methylene proton hyperfine components in Figure 8B are the line pair 7,7′ and the weak shoulders 10,10′ with corresponding values of $A_1 = 5.8$ MHz and $A_2 = 9.2$ MHz. When these values are assigned to the $A_\perp$ and $A_\parallel$ components of one methylene proton, the resulting isotropic value A_{iso} is 7.5 MHz. Recent ENDOR experiments on $Q_A^{\bullet-}$ in single crystals of bacterial reaction centers yielded a similar isotropic value and hyperfine anisotropy for one methylene β-proton, whereas the second proton hfc is found to be quite small (Isaacson et al., 1995a).

Comparison with PQ-9$^{\bullet-}$ indicates that the A_{XX} and A_{ZZ} hyperfine components of the α-proton (position 6) probably also contribute in the spectral range of lines 9 and 10 (9′ and 10′). They are however not resolved, presumably due to overlap with the methyl and methylene lines and due to their low intensity resulting from the large anisotropy.

Q-Band (35 GHz) EPR Characterization of $Q_A^{\bullet-}$. The iron-depleted PS II samples measured at X-band frequencies exhibit broad, unresolved Gaussian envelope EPR spectra yielding only an average g-factor and line width (see Table 3). In order to resolve the **g**-tensor, it is necessary to use higher microwave frequencies.

The Q-band EPR spectra of $Q_A^{\bullet-}$ in iron-depleted D_2O-exchanged PS II and of PQ-9$^{\bullet-}$ in 2-propanol-d_8 are shown in Figure 9 together with computer simulations. The principal values of the **g**-tensors of both species are collected in Table 5. A surprisingly large difference occurs for the g_{XX} value.

The **g**-tensor of a quinone anion radical is influenced by the spatial distribution of the orbital carrying the unpaired electron and is thus strongly influenced by the π-spin densities at the carbonyl oxygens, which have a much larger spin orbit coupling constant as compared with carbon (Carrington & McLachlan, 1967). The g_{XX} component, which lies along the C−O bond direction, has been shown to be extremely sensitive to environmental effects near the oxygen atoms (Burghaus et al., 1993). To first order the dominant contribution to $\Delta g_{XX} = |g_{XX} - g_e|$ is associated with the excitation of an electron from the lone-pair (n, nonbonding) orbital of the oxygen atoms into the half-occupied

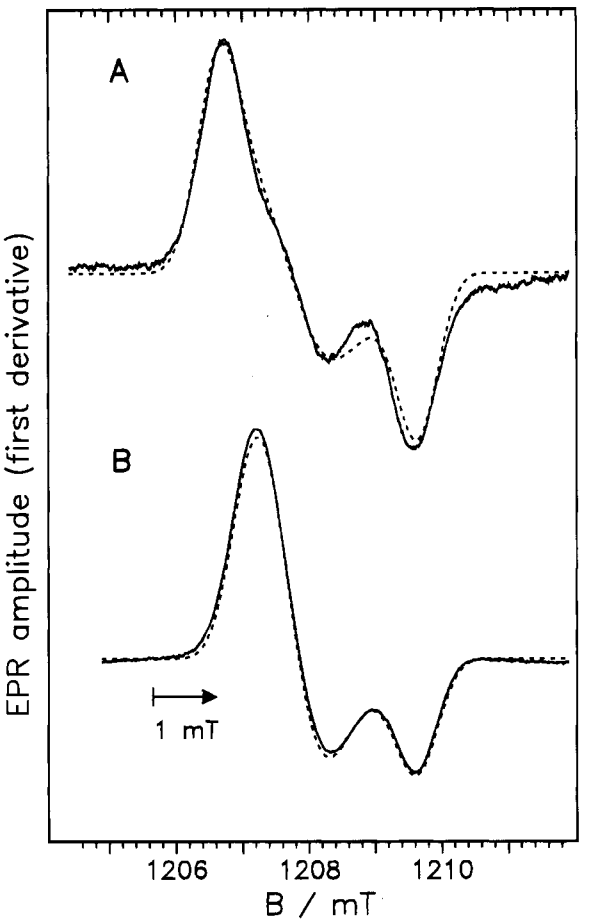

FIGURE 9: Experimental and simulated Q-band EPR spectra at 33.9 GHz. Iron-depleted PS II membrane fragment samples treated with dithionite in D_2O buffer (A) and PQ-9$^{\bullet-}$ (10^{-3} M) in alkaline 2-propanol (fully deuterated) (B). Experimental conditions: P_{MW}, 2.5 μW; field modulation depth, 0.2 mT, frequency, 12.5 kHz; accumulation time, 10 min; $T = 80$ K; PS II sample concentration, 10 mg of Chl a mL^{-1}. The dashed curves show computer simulations for both spectra using the **g** and hf tensor values given in Tables 5 and 4 and a basic line width of 0.24 mT.

Table 5: Principal Values of the **g**-Tensors of the Electron Acceptor Radical Anion $Q_A^{\bullet-}$ in PS II and in Purple Bacteria and of the Radical Anions PQ-9$^{\bullet-}$and $UQ_{10}^{\bullet-}$ in 2-Propanol ($T = 80$ K)

radical		g_{XX}	g_{YY}	g_{ZZ}	1/3 Tr g	ref
PS II	$Q_A^{\bullet-}$	2.0073	2.0054	2.0023	2.0050	*a*
	PQ-9$^{\bullet-}$	2.0063	2.0052	2.0022	2.0046	*a*
bRC	$Q_A^{\bullet-}$	2.0066	2.0054	2.0022	2.0047	*b*
	$UQ_{10}^{\bullet-}$	2.00646	2.00542	2.00222	2.00470	*b*

[a] This work; all values obtained by simulation of the powder Q-band (33.9 GHz) EPR spectra. The error is ±0.0001. [b] W-band (95 GHz) EPR measurements. The error is ±0.0001 for $Q_A^{\bullet-}$ and ±0.00005 for $UQ_{10}^{\bullet-}$ (Burghaus et al., 1993).

π^*-orbital and is inversely proportional to the energy gap ΔE between these two orbitals (Burghaus et al., 1993). The g_{XX} value of $Q_A^{\bullet-}$ is much larger than that found for PQ-$9^{\bullet-}$, indicating a difference in the environment around the Q_A oxygen atoms. An increase in Δg_{XX} can be caused by a decrease of the π^*-orbital energy, by an increase of the n orbital energy, or by increased π-spin densities at the oxygen atoms. The π^*-orbital energy may be affected by π interactions with nearby aromatic amino acid residues (π-stacking), whereas an increase of the n orbital energy can result from weaker hydrogen bonds to the quinone carbonyl oxygens. According to Scheme 1, weaker hydrogen bonding leads to increased π-spin density at the respective oxygen atom, resulting also in an increase of Δg_{XX}.

Table 5 shows a comparison of the **g**-tensor principal values of $Q_A^{\bullet-}$ in PS II and in bacterial reaction centers (Burghaus et al., 1993) together with the values of the respective isolated quinone radical anions PQ-$9^{\bullet-}$ and $UQ_{10}^{\bullet-}$ in 2-propanol. When comparing $UQ_{10}^{\bullet-}$ and $Q_A^{\bullet-}$ in the bacterial reaction center, there are two effects on g_{XX} which have opposite directions. From ENDOR experiments (Feher et al., 1985) it has been concluded that $Q_A^{\bullet-}$ has stronger hydrogen bonds than $UQ_{10}^{\bullet-}$ in 2-propanol. This should lead to a decrease of g_{XX}. Instead, a slight but significant increase of g_{XX} is observed for $Q_A^{\bullet-}$. This has been attributed to a $\pi-\pi$ interaction with the nearby Trp (M252) which decreases the energy of the π^*-orbital of $Q_A^{\bullet-}$, thereby increasing g_{XX} (Isaacson et al., 1995b). This effect obviously overcompensates the expected decrease of g_{XX} resulting from the stronger H-bonds. In the X-ray structure of the bacterial reaction center (Komiya et al., 1988) the π-plane of Trp (M252) is oriented almost parallel to that of $Q_A^{\bullet-}$ at a distance which suggests π-interaction. Calculations indicated that this π-interaction is important for electron transfer from pheophytin to Q_A (Plato et al., 1989).

For $Q_A^{\bullet-}$ in PS II we find from ENDOR weaker hydrogen bonds than for PQ-$9^{\bullet-}$ in 2-propanol. We propose that in this case both effects, the weaker H-bonds and the $\pi-\pi$ interaction with a nearby amino acid residue, sum and result in the large observed g_{XX} value (Table 5). It has been shown that a tryptophan residue (W253) in D2 close to the Q_A binding site is essential for the formation of PS II (Vermaas et al., 1990). Thus we postulate that the energy gap (ΔE) in $Q_A^{\bullet-}$ is influenced not only by a change in the hydrogen bonding to $Q_A^{\bullet-}$ but also by π-stacking with aromatic amino acid residues and that D2-W253 is a very likely candidate for this.

Since the present study was performed on iron-depleted PS II preparations, it is not clear whether the observed weaker hydrogen bonds of $Q_A^{\bullet-}$ in PS II, as compared with purple bacteria, are also weaker in the untreated native PS II. However, based on the unchanged kinetics of the electron transfer from pheophytin to Q_A, we assume no *major* structural changes for Q_A in the iron-depleted preparations.

SUMMARY

The aim of this paper was the elucidation of the electronic structure of the electron acceptor Q_A in photosystem II (PS II). The influence of the protein surrounding on the spin density distribution in the anion radical ($Q_A^{\bullet-}$) was of special interest. An attempt has been made to characterize the $Q_A^{\bullet-}$ binding site in the protein matrix by comparison of the **g**-tensor and hyperfine couplings of isolated PQ-$9^{\bullet-}$ *in vitro* with those of $Q_A^{\bullet-}$ *in vivo* using EPR and ENDOR spectroscopy, respectively.

For PQ-$9^{\bullet-}$ the investigation yielded a complete set of isotropic g-values and isotropic hyperfine coupling constants in liquid solution. The latter were assigned to molecular positions by using TRIPLE resonance techniques and their temperature dependences and by comparison with MO calculations. From frozen solutions of both protonated and deuterated solvents two methyl group hyperfine tensors and two different hyperfine tensors from hydrogen bond protons were obtained, respectively.

The different magnitudes both of the two methyl hyperfine tensors (positions 2 and 3, Figure 1) and of the two hydrogen bond protons strongly suggest an asymmetrical hydrogen bonding with the stronger (and hence shorter) bond to oxygen O_1. The weaker hydrogen bond to O_4 may result from steric hindrance due to the isoprenyl chain at position 5.

$Q_A^{\bullet-}$ was generated either chemically with sodium dithionite or photochemically. Using Q-band EPR spectroscopy the **g**-tensors of $Q_A^{\bullet-}$ and PQ-$9^{\bullet-}$ were determined by computer simulations. The results showed a noticeable difference in one of the **g**-tensor components (g_{XX}). This shift indicates weaker hydrogen bonds in $Q_A^{\bullet-}$ and possible π-interaction with nearby aromatic amino acid residues.

Using ^{1}H-ENDOR spectroscopy, the hyperfine structure of $Q_A^{\bullet-}$ in PS II was resolved for the first time. The spectrum showed similarities to that of PQ-$9^{\bullet-}$ in frozen solution. However, differences in the measured methyl hyperfine couplings reflect a somewhat altered spin density distribution in $Q_A^{\bullet-}$. D_2O/H_2O exchange was used to identify two hydrogen bond tensors, one of them being weaker than that in PQ-$9^{\bullet-}$ in frozen 2-propanol.

Both the hf tensor components of the methyl protons at positions 2 and 3 and those assigned to the hydrogen bond protons show that for $Q_A^{\bullet-}$ in the protein matrix an asymmetric hydrogen bonding is present. This asymmetry is probably caused by two factors, the shielding effect of the bulky isoprenoid chain, which is also present in PQ-$9^{\bullet-}$ *in vitro*, and the specific amino acid environment in the protein. The data in this study further indicate that the stronger hydrogen bond assigned to O_1 is somewhat weaker than in PQ-$9^{\bullet-}$ *in vitro*, while the second hydrogen bond assigned to O_4 is of similar strength in both cases. The large g_{XX} component of $Q_A^{\bullet-}$ as compared with PQ-$9^{\bullet-}$ measured in Q-band EPR spectra furthermore indicates a π-interaction with a nearby aromatic amino acid residue. A possible candidate is Trp (M253), which has been shown by site-specific mutagenesis to be essential for assembly of PS II (Vermaas et al., 1990).

Our data show that the hydrogen-bonding situation of $Q_A^{\bullet-}$ in PS II is somewhat altered with respect to PQ-$9^{\bullet-}$ in frozen alcoholic solution but is similar to that of $Q_A^{\bullet-}$ in bacterial reaction centers, where asymmetric hydrogen bonding has been established from ENDOR on D_2O/H_2O-exchanged samples and from EPR on ^{17}O-enriched $Q_A^{\bullet-}$ (Feher et al., 1985). In a recent EPR study, where Q_A has been replaced by UQ_{10}, which was selectively enriched in ^{13}C, a stronger hydrogen bond was reported for O_4 and was tentatively assigned to His M219, which is a ligand to Fe^{2+} (van den Brink et al., 1994). The hydrogen bonds of $Q_A^{\bullet-}$ in iron-depleted PS II are, however, weaker than those of $Q_A^{\bullet-}$ in

bacterial reaction centers. In purple bacteria π-interaction between Q_A and a nearby Trp (M252) is suggested by the X-ray structure (Komiya et al., 1988) and has been shown by site-directed mutagenesis to strongly influence the electron-transfer rates from bacteriopheophytin to Q_A (Stilz et al., 1994).

The data presented in this study reveal a close similarity of the binding site of $Q_A^{\bullet-}$ in PS II and $Q_A^{\bullet-}$ in bacterial reaction centers.

Recently it has been shown that $Q_A^{\bullet-}$ can also be generated in PS II membrane fragments which have been treated with cyanide. It was proposed that ligation of Fe^{2+} by cyanide leads to the formation of low-spin ($S = 0$) Fe^{2+} (Sanakis et al., 1994). Preliminary Q-band EPR and ENDOR experiments performed in our laboratory indicate structural changes of the $Q_A^{\bullet-}$ site in these preparations as compared with the iron-depleted samples investigated here. In certain PS II core preparations (Adir et al., 1992) $Q_A^{\bullet-}$ also seems to be decoupled from Fe^{2+}. These preparations are particularly interesting with respect to possible crystallization. Work is in progress to further characterize $Q_A^{\bullet-}$ and its microenvironment in these preparations.

ACKNOWLEDGMENT

The authors are grateful to Prof. Dr. H. Kurreck (Freie Universität Berlin) for the use of his spectrometer for some of the initial measurements. J. Kurreck, M. Müller, K. Scharf, and B. Lange are acknowledged for their help with the PS II sample preparations; Dr. R. Bittl and W. Zweygart are acknowledged for the ENDOR software; W. Zweygart, for the Q-band EPR software; and R. Fiege, for the EPR powder simulation program (all from the Technische Universität Berlin). Furthermore, we would like to thank Dr. L.-E. Andréasson (Chalmers University, Göteborg) for assistance with the helium temperature EPR measurements of $Q_A^{\bullet-}Fe^{\bullet 2+}$ and Dr. M. Plato (Freie Universität Berlin) for his support with the MO calculations. Professor A. Müller (University of Bielefeld) is thanked for the ICP mass spectrometry measurements. Dr. H.-J. Eckert and Dr. A. Napiwotzski (Technische Universität Berlin) provided the optical data.

REFERENCES

Adir, N., Okamura, M. Y., & Feher, G. (1992) *Research in Photosynthesis* (Murata, N., Ed.) Vol. 2, pp 195−198, Kluwer Academic Publishers, Dordrecht..

Atkinson, Y. E., & Evans, M. C. W. (1983) *FEBS Lett. 159*, 141−144.

Barr, R., & Crane, F. L. (1971) *Methods Enzymol. 23*, 372−408.

Bernarding, J., Eckert, H.-J., Eichler, H. J., Napiwotzski, A., & Renger, G. (1994) *Photochem. Photobiol. 59*, 566−573.

Berthold, D. A., Babcock, G. T., & Yocum, C. F. (1981) *FEBS Lett. 134*, 231−234.

Biehl, R., Plato, M., & Möbius, K. (1975) *J. Chem. Phys. 63*, 3515.

Bowden, S. J., Hallahan, B. J., Ruffle, S. V., Evans, M. C. W., & Nugent, J. H. A. (1991) *Biochim. Biophys. Acta 1060*, 89−96.

Bowes, J. M., Crofts, C. A., & Itoh, S. (1979) *Biochim. Biophys. Acta 547*, 320−335.

Burghaus, O. (1991) Doctoral Thesis, Physics Department, Freie Universität Berlin (in German).

Burghaus, O., Plato, M., Rohrer, M., Möbius, K., MacMillan, F., & Lubitz, W. (1993) *J. Phys. Chem. 97*, 7639−7647.

Carrington, A., & McLachlan, A. D. (1967) *Introduction to Magnetic Resonance*, Chapman and Hall, London.

Conjeaud, H., Mathis, P., & Paillotin, G. (1979) *Biochim. Biophys. Acta, 546*, 280−291.

Crofts, A. R., & Wraight, C. A. (1983) *Biochim. Biophys. Acta 726*, 149−185.

Das, M. R., Connor, H. D., Lenairt, D. S., & Freed, J. H. (1970) *J. Am. Chem. Soc. 92*, 2258−2268.

Debus, R. J., Feher, G., & Okamura, M. Y. (1986) *Biochemistry 25*, 2276−2287.

Deisenhofer, J., & Michel, H. (1988) *EMBO J. 8*, 2149−2170.

Dinse, K. P., Biehl, R., & Möbius, K. (1974) *J. Chem. Phys. 61*, 4335.

Eckert, H.-J., Wydrzynski, T., & Renger, G. (1988a) *Biochim. Biophys. Acta 932*, 240−249.

Eckert, H.-J., Wiese, N., Bernading, J., Eichler, H. J., & Renger, G. (1988b) *FEBS Lett. 240*, 153−158.

Feher, G., & Okamura, M. Y. (1978) in *The Photosynthetic Bacteria* (Clayton, R. K., & Sistrom, W. R., Eds.) pp 339−386, Plenum Press, New York.

Feher, G., Isaacson, R. A., Okamura, M. Y., & Lubitz, W. (1985) *Springer Ser. Chem. Phys. 42*, 174−189.

Feher, G., Allen, J. P., Okamura, M. Y., & Rees, D. C. (1989) *Nature 339*, 111−116.

Govindjee and van Rensen, J. J. S. (1994) in *The Photosynthetic Reaction Center* (Deisenhofer, J., & Norris, J. R., Eds.) pp 357−389, Academic Press, San Diego.

Haag, E., Gleiter, H. M., & Renger, G. (1992) *Photosynth. Res. 31*, 113−126.

Hyde, J. S., Rist, G. H., & Ericksson, L. E. G. (1968) *J. Phys. Chem. 72*, 4269−4276.

Isaacson, R. A., Abresch, E., Feher, G., Lubitz, W., Williams, J. C., & Allen, J. P. (1995a) *Biophys. J. 68* (2), A246 (abstract).

Isaacson, R. A., Lendzian, F., Abresch, E. C., Lubitz, W., & Feher, G. (1995b) *Biophys. J.* (in press).

Käss, H., Rautter, J., Zweygart, W., Struck, A., Scheer, H., & Lubitz, W. (1994) *J. Phys. Chem. 98*, 354−363

Klimov, V. V., Dolan, E., Shaw, E. R., & Ke, B. (1980) *Proc. Natl. Acad. Sci. U.S.A. 77*, 7227−7231.

Kohl, D. H., Wright, J. R., & Weissman, M. (1969) *Biochim. Biophys. Acta 180*, 536−544.

Komiya, H., Yeates, T. O., Rees, D. C., Allen, J. P., & Feher, G. (1988) *Proc. Natl. Acad. Sci. U.S.A. 85*, 9012−9016.

Kurreck, H., Kirste, B., & Lubitz, W. (1988) *Electron Nuclear Double Resonance Spectroscopy of Radicals in Solution*, VCH Publishers, Inc., Weinheim.

Lichtenthaler, H. K., & Prenzel, U. (1977) *J. Chromatogr. 135*, 493−498.

Lubitz, W. (1991) in *Chlorophylls* (Scheer, H., Ed.) pp 903−944, CRC Press, Boca Raton, FL.

Lubitz, W., Abresch, E. C., Debus, R. J., Isaacson, R. A., Okamura, M. Y., & Feher, G. (1985) *Biochim. Biophys. Acta 808*, 464−469.

MacMillan, F. (1993) Doctoral Thesis, Chemistry Department, Freie Universität Berlin.

MacMillan, F., Gleiter, H., Renger, G., & Lubitz, W. (1990) in *Current Research in Photosynthesis* (Baltscheffsky, M., Ed.) Vol. 1, pp 531−534, Kluwer Academic Publishers, Dordrecht.

Michel, H., & Deisenhofer, J. (1988) *Biochemistry 27*, 1−7.

Napiwotzski, A. (1990) Diploma Thesis, Physics Department, Technische Universität Berlin (in German).

Nugent, J. H. A., Diner, B. A., & Evans, M. C. W. (1981) *FEBS Lett. 124*, 241−244.

O'Malley, P. J., & Babcock, G. T. (1986) *J. Am. Chem. Soc. 108*, 3995−4001.

O'Malley, P. J., Chandrashekar, T. K., & Babcock, G. T. (1985) *Springer Ser. Chem. Phys. 42*, 339−344.

Pedersen, J. A. (1978) *Phytochemistry 17*, 775−778.

Pederson, J. B., Hansen, C. E. M., Parbo, H., & Muus, L. T. (1975) *J. Chem. Phys. 63*, 2398−2405.

Petrouleas, V., & Diner, B. A. (1986) *FEBS Lett. 147*, 111−114.

Plato, M., Michel-Beyerle, M. E., Bixon, M., & Jortner, J. (1989) *FEBS Lett. 249*, 70−74.

Plato, M., Möbius, K., & Lubitz, W. (1991) in *Chlorophylls* (Scheer, H., Ed.) pp 1015−1046, CRC Press, Boca Raton, FL.

Press, W. H., Flannery, B. P., Teukolsky, S. A., & Vetterling, W. T. (1988) in *Numerical Recipies,* Cambridge University Press, Cambridge.

Renger, G. (1972) *Biochim. Biophys. Acta 256*, 428−439.

Renger, G. (1976) *Biochim. Biophys. Acta 440*, 287−300.

Renger, G. (1993) *Photosynth. Res. 38*, 229−247.
Renger, G., Völker, M., & Weiss, W. (1984) *Biochim. Biophys. Acta 766*, 582−591.
Renger, G., Rutherford, A. W., & Völker, M. (1985) *FEBS Lett. 185*, 243−247.
Renger, G., Wacker, U., & Völker, M. (1987) *Photosynth. Res. 13*, 167−189.
Renger, G., Hanssum, B., Gleiter, H. M., Koike, H., & Inoue, Y. (1988) *Biochim. Biophys. Acta 936*, 435−446.
Rieger, P. H. (1982) *J. Magn. Reson. 50*, 485−489.
Rigby, S. E. J., Nugent, J. H. A., & O'Malley, P. J. (1994) *Biochemistry 33*, 10043−10050.
Rist, G. H., & Hyde, J. S. (1970) *J. Chem. Phys. 52*, 4633−4643.
Rohrer, M., Plato, M., MacMillan, F., Grishin, Y., Lubitz, W., & Möbius, K. (1995) *J. Magn. Reson.* (in press).
Rutherford, A. W., & Zimmermann, J.-L. (1984) *Biochim. Biophys. Acta 767*, 168−175.
Rutherford, A. W., Zimmermann, J.-L., & Mathis, P. (1984) *FEBS Lett. 105*, 156−162.
Sanakis, Y., Petrouleas, V., & Diner, B. A. (1994) *Biochemistry 33*, 9922−9928.
Stilz, H. U., Finkele, U., Holzapfel, W., Lauterwasser, C., Zinth, W., & Oesterhelt, D. (1994) *Eur. J. Biochem. 223*, 233−242.
Trebst, A. (1986) *Z. Naturforsch. 41c*, 240−245.
Trebst, A. (1991) *Z. Naturforsch. 46c*, 557−562.
van den Brink, J. S., Spoyalov, A. P., Gast, P., van Liemt, W. B. S., Raap, J., Lugtenburg, J., & Hoff, A. J. (1994) *FEBS Lett. 353*, 273−276.
Vass, I., & Styring, S. (1991) *Biochemistry 30*, 830−839.
Vermaas, W. F. J., & Rutherford, A. W. (1984) *FEBS Lett. 175*, 243−248.
Vermaas, W. F. J., Charité, J., & Shen, G. (1990) *Z. Naturforsch. 45c*, 359−365.
Vermaas, W. F. J., Vass, I., Eggers, B., & Styring, S. (1994) *Biochim. Biophys. Acta 1184*, 263−272.
Völker, M., Ono, T., Inoue, Y., & Renger, G. (1985) *Biochim. Biophys. Acta 806*, 25−34.
Völker, M., Renger, G., & Rutherford, A. W. (1986) *Biochim. Biophys. Acta 851*, 424−430.
Weiss, W., & Renger, G. (1986) *Biochim. Biophys. Acta 850*, 173−183.
Zweygart, W., Thanner, R., & Lubitz, W. (1994) *J. Magn. Reson., Ser. A 109*, 172−177.

BI942968B